Structural Engineering and Mechanics, *Vol. 73, No. 5 (2020) 529-542*
DOI: https://doi.org/10.12989/sem.2020.73.5.529

Estimation of the load-deformation responses of flanged reinforced concrete shear walls

Bin Wang*[1,2], Qing-Xuan Shi[1,2], Wen-Zhe Cai[1] and YI-Gong Peng[1]

[1]*State Key Laboratory of Green Building in Western China, Xi'an University of Architecture and Technology, Xi'an 710055, Peoples R China*
[2]*School of Civil Engineering, Xi'an University of Architecture and Technology, Xi'an, 710055, Peoples R China*

(Received July 25, 2019, Revised October 16, 2019, Accepted October 28, 2019)

Abstract. As limited well-documented experimental data are available for assessing the attributes of different deformation components of flanged walls, few appropriate models have been established for predicting the inelastic responses of flanged walls, especially those of asymmetrical flanged walls. This study presents the experimental results for three large-scale T-shaped reinforced concrete walls and examines the variations in the flexural, shear, and sliding components of deformation with the total deformation over the entire loading process. Based on the observed deformation behavior, a simple model based on moment-curvature analysis is established to estimate flexural deformations, in which the changes in plastic hinge length are considered and the deformations due to strain penetration are modeled individually. Based on the similar gross shapes of the curvature and shear strain distributions over the wall height, a proportional relationship is established between shear displacement and flexural rotation. By integrating the deformations due to flexure, shear, and strain penetration, a new load-deformation analytical model is proposed for flexure-dominant flanged walls. The proposed model provides engineers with a simple, accurate modeling tool appropriate for routine design work that can be applied to flexural walls with arbitrary sections and is capable of determining displacements at any position over the wall height. By further simplifying the analytical model, a simple procedure for estimating the ultimate displacement capacity of flanged walls is proposed, which will be valuable for performance-based seismic designs and seismic capacity evaluations.

Keywords: flanged walls; cyclic test; deformation; analytical model; ultimate displacement

1. Introduction

Reinforced concrete (RC) shear walls are typically used in high-rise buildings as primary lateral load resisting elements because of their large in-plane stiffness and strength, which enables them to carry large lateral loads due to earthquakes while also minimizing lateral displacements (Lu and Huang 2014, Parulekar *et al.* 2016, Zhao *et al.* 2017, Sakr *et al.* 2017). However, investigations into structural damage caused by recent earthquakes indicate that the inadequate deformation capacity and energy dissipation capacity of shear walls are the critical factors leading to structural failure and collapse. The application of a performance-based seismic design scheme is an effective way to control the structural response and damage degree, and accurate deformation capacity estimations are the basis of displacement-based seismic design (Varughese *et al.* 2015). Furthermore, correct prediction of the entire load versus deformation response is of major importance to seismic performance evaluation using the capacity spectrum method.

The plastic hinge model proposed by Paulay and Priestley (1992) is widely accepted and used in estimating the deformation capacity of RC shear walls because this model is simple and produces good flexural deformation estimates (Choi *et al.* 2004, Takahashi *et al.* 2013, Kang and Kim 2014, Zhou *et al.* 2014). They allow the calculation of a bilinear load-deformation relationship by separating the elastic portion of the deformation from the inelastic portion, and lumping the inelastic portion of deformation into a plastic hinge at the critical section (Grammatikou *et al.* 2019). Hence, a correct estimate of the plastic hinge length affected by shear and strain penetration dominates the accuracy of the plastic hinge model (Massone and Alfaro 2016). However, the inherent shortcomings of the plastic hinge model are that the contributions of shear and sliding deformations to lateral displacements cannot be taken into account. Therefore, combining the plastic hinge model with the truss model proposed by Park and Paulay (1975) has become a common method for considering the contribution of shear deformation (Massone *et al.* 2006, Zhang *et al.* 2009). Nevertheless, when using the truss model to calculate shear deformation, the shear stiffness is assumed to be a certain value over the entire plastic range, causing the calculated shear deformation to remain unchanged once the yield limit has been reached, which is significantly different from the observed experimental results.

For functionality and architectural reasons, symmetrical linear walls are often joined or arranged in orthogonal directions to form asymmetrical (T- and L-shaped) flanged walls (Kabir and Vasheghani-Farahani 2009, Chen *et al.* 2016). The contribution of the flange vertical reinforcement in flexural strength may result in a higher proportion of shear deformation (Bafti *et al.* 2019). Extensive

*Corresponding author, Ph.D.
E-mail: wangbin@xauat.edu.cn

http://www.techno-press.com/journals/sem&subpage=7
ISSN: 1225-4568 (Print), 1598-6217 (Online)

experimental studies on flexure-dominant flanged walls have shown that shear deformation constitutes more than 15% of the lateral top displacement and increases with increasing flexural deformation in the plastic range (Thomsen and Wallace 2004, Beyer *et al.* 2008, Wang *et al.* 2018). Therefore, neglecting the shear deformation contribution or assuming constant shear stiffness will underestimate the deformation capacity of flanged walls.

Due to the unclear shear mechanism and the complexity in flexure-shear interaction, estimation of the shear deformation has been a difficult issue in predicting the inelastic response of RC shear walls. Although considerable numbers of studies have been performed to account for nonlinear shear deformation, but most of these efforts concerned rectangular walls (Hossain and Wright 2004). Dazio *et al.* (1999) examined the shear deformation for displacement demands through quasi-static cyclic tests on six rectangular RC walls and found that the shear-to-flexural displacement ratio remained approximately constant for the peak displacements of all cycles in the inelastic range. Based on this observation and assuming a fanning crack pattern, empirical equations for estimating the shear-to-flexural displacement ratio were developed, and formulas for determining the ultimate displacement of flexure-dominant RC shear walls were further established combing the plastic hinge model (Hines *et al.* 2004, Priestley *et al.* 2007, Beyer *et al.* 2011). However, these methods are achieved by determining the uncertain cracking angle, which may amplify the variation in the calculation results. To account for combined axial, flexural, and shear effects, Mostafaei and Vecchio (2008) developed a uniaxial shear-flexure model to predict the full load-deformation relationships of RC elements, and Dang *et al.* (2014) applied this model to fiber-reinforced concrete shear walls. Furthermore, using the microplane concept, Hua and Yahya (2010) formulated a fiber element to model nonlinear shear deformations in medium-rise RC walls, and this model can include nonlinear axial-flexural-shear interactions at the material level. Nevertheless, these methods require a relatively intensive computation and iteration process, which might be suitable for nonlinear analysis by researchers but not for structural design by engineers. More importantly, the feasibility of using the established models to predict the deformation capacity of flanged walls is debatable.

Given the deficient study on modeling the inelastic response of flanged RC walls, additional research efforts are required to establish a simple model that enables reasonable estimations of each deformation component and accurate predictions of the entire load versus deformation response with low computational cost. In this study, experimental results for three large-scale T-shaped RC walls are presented to examine the variation in each deformation component with the total deformation over the entire loading process. Based on the observed deformation behavior and using flexural section analysis, simple methods are established to estimate the flexural, shear, and strain penetration components of deformation. By integrating the three deformation components, a new load-deformation analytical model for flexure-dominant flanged walls is proposed that accounts for the contribution of deformations due to flexure, shear, and strain penetration. By further simplifying the analytical model, a simplified procedure is proposed for estimating the ultimate displacement capacity of flanged walls, which will be valuable for performance-based seismic designs and seismic capacity evaluations.

2. Experimental program and observations

2.1 Specimens *and testing*

Three large-scale T-shaped RC wall specimens with different detailing at boundaries were tested under combined constant axial loading and reversed cyclic lateral loading. The specimen details are listed in Table 1. The three wall specimens are 2200 mm tall and 100 mm thick with a web length of 1000 mm and a flange length of 900 mm. The configuration and reinforcement details of all three specimens (TW-1, TW-3 and TW-4) are shown in Fig. 1. The wall specimens were designed with adequate shear reinforcement and favorable anchorage conditions to ensure flexural domination and to prevent shear, sliding and anchorage failures. Fine aggregate concrete with a mean compressive strength of 32.3 MPa was used for all specimens. Hot-rolled deformed bars were used as web

Table 1 Specimen parameters

Specimens	Boundary confinement at the web-flange intersection	Range of the web boundary region (mm)	Longitudinal bars at the web boundary	Transverse bars at the web boundary	V_N[a]	V_{MAX}[b]	θ_U[c]
TW-1	Yes	240	8-Ø10[d]	Ø6@75[e]	489 -489	380 -216	1/88 -1/48
TW-3	Yes	320	10-Ø10	Ø6@50	489 -489	387 -231	1/68 -1/41
TW-4	No	240	8-Ø10	Ø6@75	489 -489	322 -217	1/78 -1/47

* a Nominal shear capacity (flange in tension/flange in compression).
* b Maximum applied lateral load.
* c Ultimate drift ratio
* d Number of longitudinal bars - bar diameter in mm.
* e Bar diameter in mm @ bar spacing in mm.

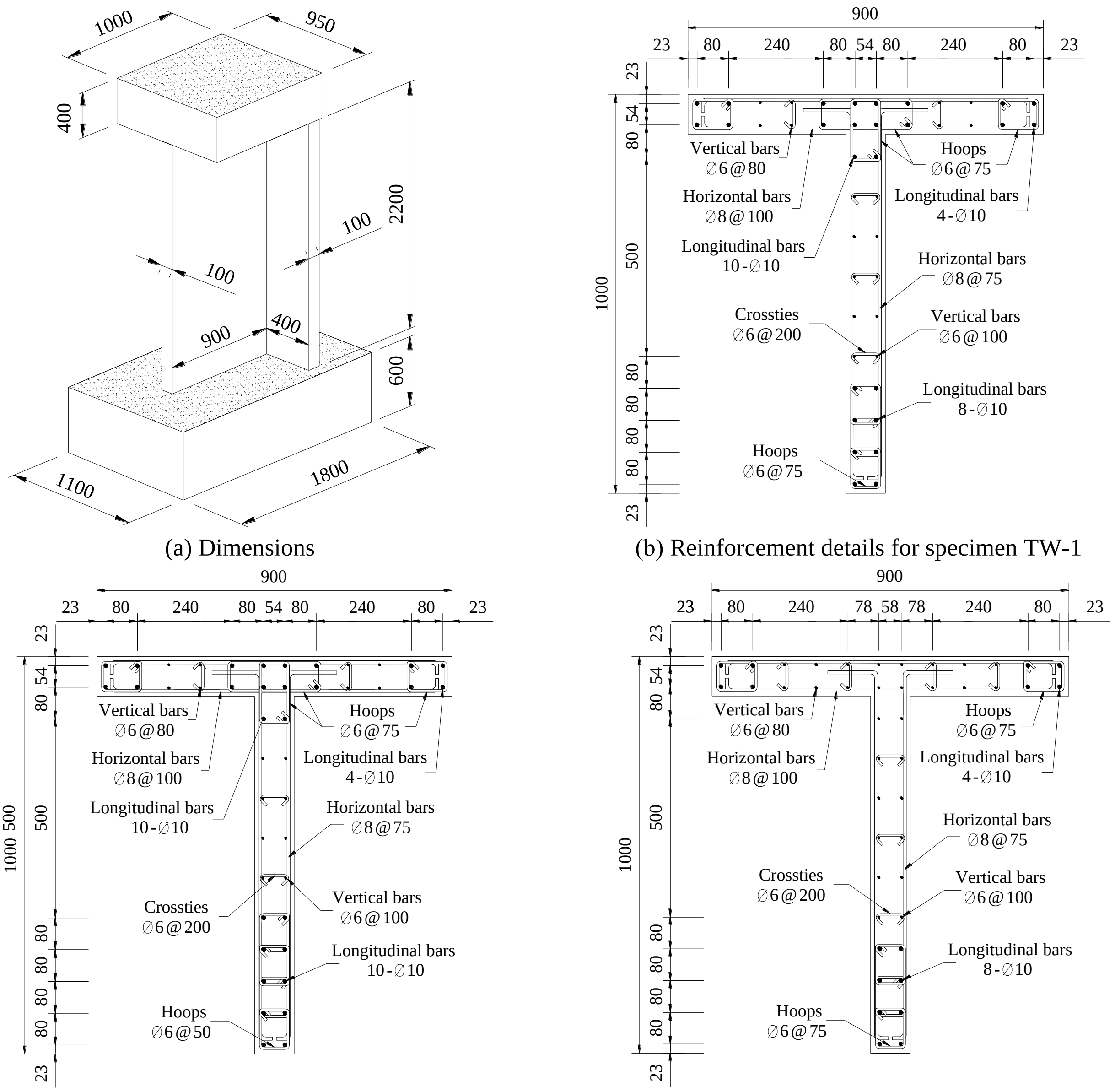

(a) Dimensions (b) Reinforcement details for specimen TW-1

(c) Reinforcement details for specimen TW-3 (d) Reinforcement details for specimen TW-4

Fig. 1 Specimen configuration and reinforcement details

Table 2 Reinforcing steel properties

Rebar type	Rebar grade	Diameter d (mm)	Yield strength f_y (MPa)	Ultimate strength f_u (MPa)	Elongation δ_u (%)
Longitudinal reinforcement	HRB400	10	478	610	21.5
Distributed horizontal reinforcement	HRB335	8	540	723	20.5
Distributed vertical reinforcement	HRB335	6	423	564	21.5
Transverse reinforcement	HRB335	6	408	582	20

reinforcement and longitudinal reinforcement, whereas hot-rolled plain bars were used as transverse reinforcement. The properties of the reinforcing steel are listed in Table 2. More detailed experimental information is available elsewhere (Wang *et al*. 2018).

A cantilever loading device was adopted for this test, as shown in Fig. 2. An axial load of approximately $0.10A_g f_c'$ was applied to the top of the wall by hydraulic jacks. Cyclic lateral displacements with unequal amplitudes were applied to the wall by a hydraulic actuator to allow the asymmetrical specimens to be loaded to failure in two loading directions (flange in tension and flange in compression). Failure of the specimens was defined at the displacement associated with a decrease in moment resistance to 85% of the maximum measured value.

To accurately measure the deformation process, a high-precision non-interference measurement method based on particle image velocimetry (PIV) was adopted to decouple the total deformation into flexural, shear and sliding deformations, as shown in Fig. 3. This technique combines digital photography, close-range photogrammetry and

Fig. 2 Test setup

Fig. 3 Measuring device based on the PIV technique

image analysis by PIV and can measure the changes in the location of any control point (target markers) on the specimen. The specific measurement system used for the PIV technique and the procedure for decoupling the deformations using this technique are detailed in Wang *et al.* (2019a).

2.2 Deformation analysis

The total top displacement of a cantilever RC wall can be interpreted as the sum of flexural deformations Δ_f, shear deformations Δ_s and sliding deformations Δ_{sl}. To investigate the variation in each deformation component with the total deformation for flexure-dominant flanged walls, Fig. 4 shows the relative contributions of different deformation components to the total displacement at various loading steps for all three specimens. Additionally, Fig. 4 also compare the total displacements Δ_{PIV} obtained by summing the three deformation components derived from the PIV technique with the top displacements Δ_{LVDT} measured using linear variable differential transformers (LVDTs), in the form of $\Delta_{PIV}/\Delta_{LVDT}$ ratios. The $\Delta_{PIV}/\Delta_{LVDT}$ ratios varied within 0.9 to 1.1 for different loading steps, which verified the accuracy of the deformations measured by the PIV technique.

The sliding deformations between the wall and the foundation did not exceed 10% of the total displacement in the initial loading stage. With the increase in top displacement, the sliding deformations contributed a decreasing proportion of the total displacement. Over the entire plastic range, the sliding deformations were less than 3% of the total displacement in the flange-in- tension loading direction, whereas the sliding deformations were only approximately 1% of the total displacement in the flange-in-compression loading direction. Therefore, the contribution of sliding deformations can be neglected in the calculation of deformation capacity.

The shear deformations accounted for a relatively higher proportion of the total displacement before concrete cracking. With the continuous development of flexural cracks at the bottom of the web, the increase in flexural deformations was faster than that of shear deformations, resulting in a significant decrease in the shear-to-total deformation ratio. Then, as the original flexural cracks developed obliquely into diagonal cracks, the decreasing trend of the shear-to-total deformation ratio gradually slowed. As the drift level increased beyond the yielding point, the shear deformations increased in proportion to the flexural deformations. Since the sliding deformations are too small to be neglected, it is concluded that for flexure-dominant T-shaped walls without significant damage to the shear-transfer mechanism, the shear-to-total deformation ratio remains approximately constant over the entire plastic range. In addition, the shear deformations accounted for 10% to 14% of the total displacement in the flange-in-tension loading direction and reached 13% to 17% of the total displacement in the flange-in-compression loading direction. Therefore, the contribution of shear deformations should be included in the calculation of deformation capacity.

3. Model for flexural deformation

The flexural deformations Δ_f can be interpreted as the sum of the flexural deformations of the wall panel $\Delta_{f,f}$ and the displacement $\Delta_{f,\theta}$ due to the fixed-end rotation of the wall associated with the strain penetration of the longitudinal reinforcing bars into the foundation. Different models are established for each of these two components.

3.1 Flexural deformation of the wall panel

For a cantilever wall component subjected to a given load, the curvature distribution over the wall height can be determined based on the moment distribution using the moment-curvature relationship. Then, the flexural deformations can be obtained by integrating the curvature along the wall height twice. This method is appealing due to its clear calculation process, but large deviations will be caused in the post-peak range. These deviations occur because when the curvature of the bottom section exceeds the peak point of the moment-curvature curve (i.e., as additional displacement is applied beyond the displacement causing the maximum resistance), the curvatures above the bottom section calculated from the reduced moments are

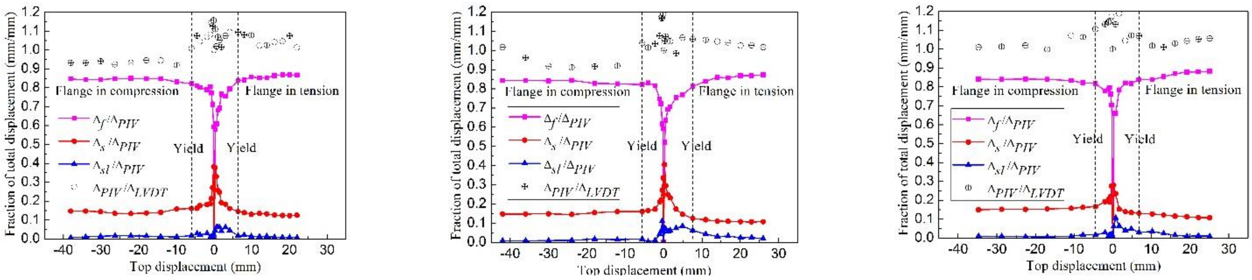

(a) TW-1 (b) TW-3 (c) TW-4

Fig. 4 Contributions of each deformation component to the total displacement in different loading steps

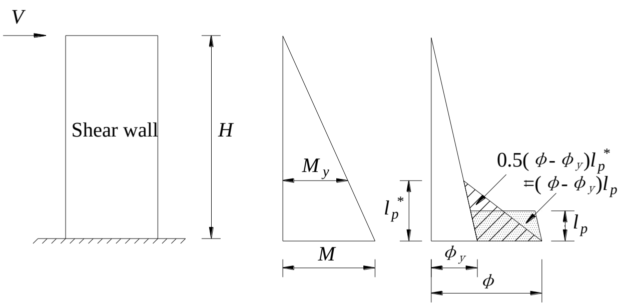

Fig. 5 Curvature distribution assumed in the plastic hinge analysis

smaller than the curvatures at the peak point and far smaller than the experimental values, thereby underestimating the flexural deformations. In addition, such a method requires high computational effort due to the complexity in determining the curvature distribution from the moment distribution. Another simple approach using the plastic hinge model allows the calculation of a bilinear load-displacement relationship based on the estimates of the plastic hinge length and curvatures at the yield and ultimate limit state. However, for the sake of simplicity, this approach generally assumes that the plastic hinge length remains constant over the entire plastic range, which also results in large differences between the calculated results and the experimental values.

Combining the advantages of the above two approaches, a piecewise calculation method based on moment-curvature analysis is adopted in this paper, and the changes in the plastic hinge length are considered. For a cantilever shear wall subjected to a concentrated force at its top surface, the lateral load can be determined by the ratio of the moment at the bottom derived from the sectional analysis to the wall height, and the displacement is calculated in two stages: pre-yielding and post-yielding ranges. In the pre-yielding range, the curvature is linearly distributed along the wall height; then, the elastic flexural deformations of the wall panel can be estimated as follows:

$$\Delta_{ef,f} = \frac{1}{3}\phi H^2 \tag{1}$$

where ϕ is the curvature of the bottom section derived from the moment-curvature analysis, and H is the wall height.

In the post-yielding range, the plastic hinge model is used to estimate the flexural deformations, but the plastic hinge length is no longer assumed to be a certain value. According to the piecewise-linear curvature profile in Fig. 5, the variable equivalent plastic hinge length l_p can be determined as follows:

$$l_p = 0.5l_p^* = 0.5H\left[1-\left(\frac{M_y}{M}\right)\right] \tag{2}$$

where l_p^* is the true plastic hinge length and M_y and M are the yield moment and the moment of each loading step derived from the moment-curvature analysis, respectively. Using Eq. (2), l_p can be accurately estimated until the ultimate moment capacity is reached. However, in the post-peak range, the plastic hinge length varied little according to the experimental observations. Therefore, the equivalent plastic hinge height at the peak moment is used to calculate the post-peak displacement. Following Hines (2002) suggestion for assessment purposes, the center of rotation for the plastic deformation is placed at the bottom of the plastic hinge region, and then the post-yield flexural deformations of the wall panel can be estimated as follows:

$$\Delta_{f,f} = \Delta_{yf,f} + \Delta_{pf,f} = \frac{1}{3}\phi_y H^2 + (\phi-\phi_y)l_p H \tag{3}$$

where $\Delta_{yf,f}$ is the yield displacement, $\Delta_{pf,f}$ is the plastic displacement, and ϕ_y is the yield curvature derived from the moment-curvature analysis.

3.2 Flexural deformation due to strain penetration

A common method to account for the contribution of deformations due to strain penetration is to add an additional equivalent plastic hinge length based on the plastic hinge model. However, such strategy lacks theoretical basis and the increased constant plastic hinge length is mostly decided by experience. More importantly, such a strategy fails to reflect the feature of the increase in the slip of the longitudinal bars with increasing top: displacement. Therefore, an individual model is used to estimate the deformations due to strain penetration in this paper. Based on the assumption that the plane sections remain plane, the rigid body rotation of a wall due to strain penetration can be calculated according to the slip of the extreme tensile bars and the neutral axis location, as shown in Fig. 6; thus, the deformations due to strain penetration can be expressed as follows:

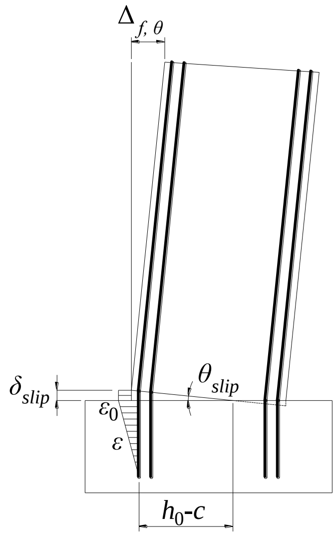

Fig. 6 Models for estimating the deformations due to strain penetration

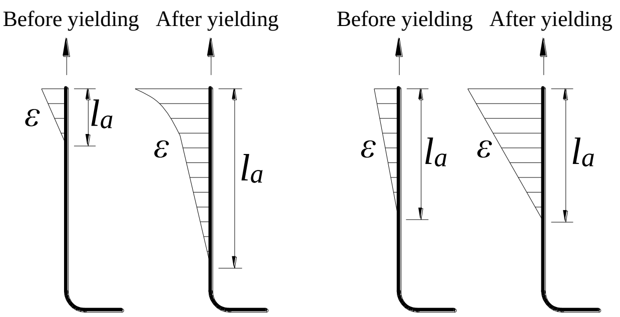

Fig. 7 Strain distributions of the tensile bars in the anchorage region

$$\Delta_{f,\,\theta} = \theta_{slip} H = \frac{\delta_{slip} H}{h_0 - c} \tag{4}$$

where θ_{slip} is the rotation due to strain penetration, δ_{slip} is the slip of the extreme tensile bars in the anchorage zone, h_0 is the effective height of the section (distance from the extreme tensile bars to the extreme compression fiber), and c is the neutral axis depth.

The neutral axis depth can be obtained directly from the moment-curvature analysis. The slip of the extreme tensile bars is determined using the model proposed by Lowes and Altoontash (2003), for which two simplifications are made to facilitate the use of this model by structural engineers. One simplification is that the anchorage length l_a is calculated corresponding to the yield stress of the tensile bars and assumed to be constant with increasing applied displacement. The other simplification is that the strain distribution over the anchorage length is assumed to be linear for any drift levels. Fig. 7 compares the actual strain distribution adopted in the model by Lowes and Altoontash to the simplified strain distribution assumed in this paper. The simplified model overestimates the slip of the tensile bars before yielding and underestimates the slip after yielding. However, the actual strain distribution should be determined by adding zero-length interface elements in the fiber model or spring elements in the three-dimensional solid model (Zhao and Sritharan 2007), which greatly increases the difficulty and complexity of the calculation process. Although the simplified model sacrifices some accuracy, the calculation process has been greatly simplified. Comparing the bar slip determined by the above two models using the following procedure, the discrepancy was relatively large in the flange-in-tension loading direction but within an acceptable range.

When calculating the anchorage length, the average bond stress τ_{avg} is assumed to be a constant according to Eligehausen *et al.* (1983), and this value can be estimated as $\tau_{avg} = 1.75\sqrt{f'_c}$. According to the static equilibrium between the pull-out force and the anchoring force of tensile bars ($\frac{\pi d^2}{4} f_y = \pi d l_a \tau_{avg}$), the anchorage length at yielding can be calculated as follows:

$$l_a = \frac{f_y d}{4\tau_{avg}} = \frac{f_y d}{7\sqrt{f'_c}} \tag{5}$$

where d and f_y are the diameter and yield stress of the longitudinal reinforcing bars, respectively, and f'_c is the concrete cylinder strength. According to the assumed triangular strain distribution, the slip of the extreme tensile bars can be determined as follows:

$$\delta_{slip} = 0.5\varepsilon_0 l_a \tag{6}$$

where ε_0 is the maximum strain in the extreme tensile bars at the wall base for a given loading, which can be determined from the moment-curvature analysis. Then, substituting Eqs. (5)-(6) into Eq. (4), the flexural deformations due to strain penetration can be calculated as follows:

$$\Delta_{\mathrm{f},\,\theta} = \frac{\varepsilon_0 f_y d H}{14\sqrt{f'_c}(h_0 - c)} \tag{7}$$

When estimating the deformations due to strain penetration, d, f_y, $f'c$, H, and h_0 are all constants that can be derived directly from the material properties and geometric parameters of the wall specimen, whereas ε_0 and c can be determined from the results of the moment-curvature analysis.

3.3 Verification of the flexural model

Fig. 8 compares the experimentally measured flexural deformations $\Delta_{f\text{-}experiment}$ for all three test specimens to the predicted values $\Delta_{f\text{-}prediction}$ obtained by summing the flexural deformations of the wall panel $\Delta_{f,\,f\text{-}prediction}$ and the deformations due to strain penetration $\Delta_{f,\theta\text{-}prediction}$. The deformations due to strain penetration increase with increasing top displacements, but their contribution to the

Table 3 Comparison between measured and predicted ultimate flexural displacements

Specimen	Ultimate flexural displacement (flange in tension)			Ultimate flexural displacements (flange in compression)		
	Measured (mm)	Predicted (mm)	Measure/Predicted	Measured (mm)	Predicted (mm)	Measure/Predicted
TW-1	25.56	23.96	1.07	37.05	43.85	0.84
TW-3	29.48	27.40	1.08	45.26	45.31	1.00
TW-4	29.16	27.29	1.07	39.93	42.03	0.95

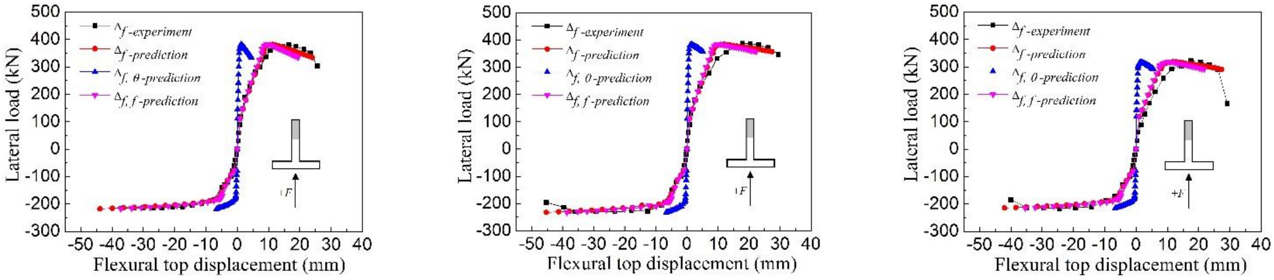

(a) TW-1 (b) TW-3 (c) TW-4

Fig. 8 Measured and predicted lateral load versus flexural top displacement relationships

total flexural deformations are within 10% over the entire loading process. The lateral load versus flexural top displacement relationships predicted by the analytical model are in good agreement with the test results except for a small deviation in the ultimate flexural displacements (Table 3). In the flange-in-tension loading direction, the predicted values of the ultimate flexural displacement are slightly smaller than the experimental values, which results from neglecting the effect of shear cracks on flexural deformations in the prediction. The development of shear cracks during the test increases the plastic hinge length, thereby increasing the flexural deformation. In the flange-in-compression loading direction, specimen failure was controlled by fracture of the buckled longitudinal bars at the free end of the web. The analytical model can calculate only the monotonic response and cannot accurately estimate the ultimate tensile strain of buckled longitudinal bars, which leads to some differences between the experimental values and the predicted values. In addition, the pre-peak stiffness of the predicted curves is greater than that of the test curves, which is also due to the reduction in bending stiffness by shear cracks. In general, the proposed model can reasonably predict the flexural response of flanged walls.

4. Model for shear deformation

Since the truss model used for estimating shear deformations is unable to consider the degradation of the shear stiffness in the plastic range and the empirical model used for estimating the shear-to-flexural deformation ratio has difficulty in determining the cracking angle, this paper attempts to combine the theoretical advantages of the truss model with the observed linear relationship between shear and flexural deformation and propose a new model for predicting the shear response of flanged walls.

4.1 Modeling *procedure*

Considering the differences in the variation in shear deformation between elastic and plastic ranges of flanged walls, two separate calculation procedures are established for pre-yielding and post-yielding ranges, respectively. Before yielding, the elastic shear deformation of a cantilever wall subjected to a concentrated force at its top surface can be estimated according to Castigliano's second theorem as follows:

$$\Delta_{es} = \mu \frac{PH}{GA_w} \tag{8}$$

where P is the applied lateral load, which can be determined from the moment-curvature analysis; G is the shear modulus; I is the cross-sectional moment of inertia of the wall; A_w is the cross-sectional area of the web; and μ is the section shape factor accounting for the uneven distribution of shear stress along the cross section. The value of μ is taken as 2.0375 according to the cross- sectional shape of the tested T-shaped wall (Shi and Liang 2012).

After yielding, the curvature is nonlinearly distributed along the wall height with large values concentrated in the plastic hinge region, and the flexural top deformations are dominated by plastic hinge rotation. Due to the interaction between flexure and shear, the shear deformations are also concentrated in the plastic hinge region despite a constant shear demand over the wall height. As a result, the gross shape of the distribution of curvatures over the wall height is similar to the gross shape of the distribution of shear strains, as Brueggen (2009) observed in the quasi-static test of T-shaped walls. Additionally, Beyer *et al.* (2011) examined the shear and axial strain distributions based on the cyclic testing of U-shaped walls and found that the magnitude of the shear strains was directly linked to the magnitude of the tensile strains in the vertical reinforcing bars. Because the neutral axis depth varies little once the boundary longitudinal bars yield (Thomsen and Wallace 2004), the tensile strains in the vertical reinforcing bars are proportional to the curvatures, which further verifies the linear relationship between shear strains and curvatures. The proportional relationship between the two values can be expressed as follows:

$$\gamma = C\phi \tag{9}$$

where γ is the shear strain and C is the proportional coefficient between the two values with units of length. Integrating both sides of Eq. (9) along the wall height leads to the proportional relationship between the shear displacement Δ_s and the flexural rotation θ_f, which is expressed as follows:

$$\Delta_s = C\theta_f \tag{10}$$

The flexural rotation θ_f has been obtained in the flexural deformation calculations mentioned above. Hence, the shear

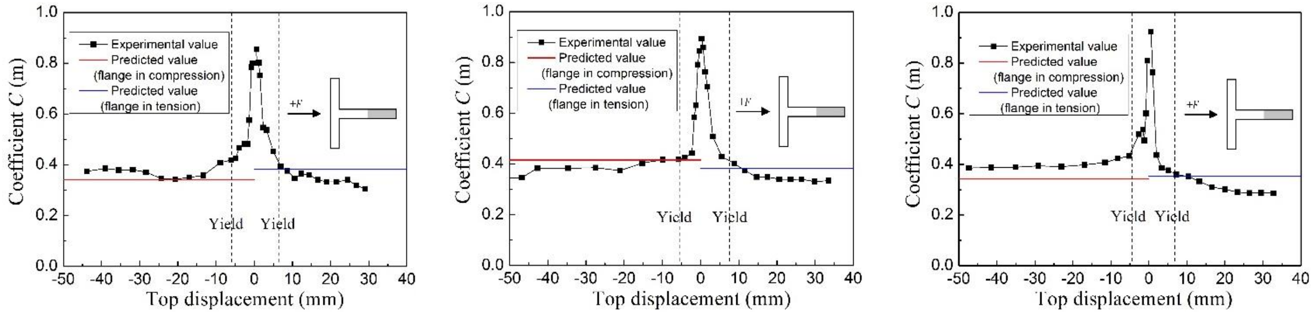

(a) TW-1 (b) TW-3 (c) TW-4

Fig. 9 Comparison of predicted coefficient C to experimental values

deformation can be calculated by simply determining the value of C.

For a given section, the curvature and shear strain can be determined by the ratio of internal force to stiffness:

$$\phi = \frac{M}{EI} \tag{11}$$

$$\gamma = \frac{V}{K_s} \tag{12}$$

where EI is the flexural stiffness, $K_s$is the shear stiffness per length, M and V are the moment and shear force (for a cantilever wall with a tip load, $M=VH$), respectively. Then, substituting Eqs. (11)-(12) into Eq. (9) yields the following expression:

$$C = \frac{EI}{K_s H} \tag{13}$$

Because the shear-to-flexural deformation ratio remains approximately constant over the entire plastic range for flexure-dominant T-shaped walls, as discussed in Section 2.2, the proportional coefficient C is assumed to be constant for all post-yielding cycles. Hence, predictions of the shear and flexural stiffness at first yielding can be used to determine the value of C. The shear stiffness can be calculated form the equation proposed by Park and Paulay (1975) on the basis of an analogous truss, which assumed the chord members as infinitely rigid and neglected shear-flexure interaction and any deformations at the anchorage of the stirrups. For simplicity of calculation, the cracking angle is assumed to be 45 degrees and the shear reinforcement is horizontally arranged according to the test, then the cracked shear stiffness per length can be calculated with thefollowing expression:

$$K_s = \frac{\rho_{sh}}{1 + 4a_E \rho_{sh}} E_s b_w h_0 \tag{14}$$

where ρ_{sh} is the ratio of the shear reinforcement area to the gross area of concrete perpendicular to that reinforcement, E_s is the elastic modulus of steel, b_w is the web width, and a_E is the ratio of the elastic modulus of steel to the elastic modulus of concrete. Considering the increase in the modular ratio a_E due to the softening of the diagonal concrete strut, a_E is taken as an average value of 10 for analysis purposes, as suggested by Priestley *et al.* (2007).

The flexural stiffness at first yielding can be calculated using the yield moment M_y and yield curvature ϕ_y derived from the moment-curvature analysis. Therefore, Eq. (13) can be written as follows:

$$C = \frac{M_y}{K_s H \phi_y} \tag{15}$$

Fig. 9 compares the coefficient C calculated using Eq. (15) to the values derived from the experimental results. For the plastic range where the proportional coefficient C needs to be used, the predicted values are closed to the test values, which verifies the accuracy of the calculation method proposed in this paper. Moreover, the values of coefficient C calculated from the test results remain approximately unchanged after the component reaches the yield limit, which further validates the assumption that the proportional coefficient C is constant for all post-yielding cycles.

Then, substituting Eq. (15) into Eq. (10) leads to the final expression of shear deformations:

$$\Delta_s = \frac{M_y}{K_s H \phi_y} \theta_f \tag{16}$$

4.2 Verification of the shear model

Fig. 10 compares the measured shear deformations in the experiment for all three test specimens to the values predicted by the analytical model. The predicted lateral load versus shear top displacement relationships closely match the measured wall responses, except for small deviations in the ultimate shear displacements (Table 4). In the flange-in-tension loading direction, the predicted values of the ultimate shear displacement are generally greater than the experimental values. This discrepancy occurs because the assumption that the shear-to-flexural deformation ratio remains constant is completely valid for the case with the flange in compression but not for the case with the flange in tension. As shown in Fig. 4, the shear-to-flexural deformation ratio tends to decrease slightly over the plastic range under positive loading, which results in the overestimation of the shear displacements. In the flange-in-compression loading direction, the predicted values of the ultimate shear displacement are slightly smaller than the experimental values. This discrepancy occurs because when calculating the cracked shear stiffness through Eq. (14), the

Table 4 Comparison between measured and predicted ultimate shear displacements

Specimen	Ultimate shear displacement (flange in tension)			Ultimate shear displacements (flange in compression)		
	Measured (mm)	Predicted (mm)	Measure/Predicted	Measured (mm)	Predicted (mm)	Measure/Predicted
TW-1	3.29	3.49	0.94	6.34	6.15	1.03
TW-3	3.54	3.74	0.95	7.82	6.66	1.17
TW-4	3.26	3.2	1.01	7.03	5.89	1.19

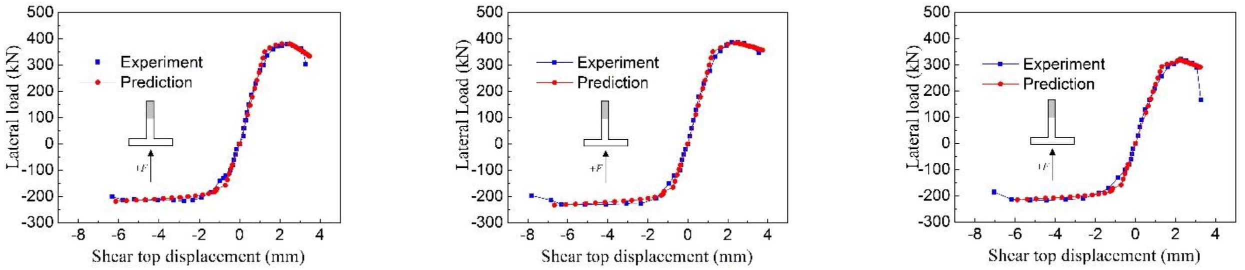

(a) TW-1 (b) TW-3 (c) TW-4

Fig. 10 Measured and predicted lateral load versus shear top displacement relationships

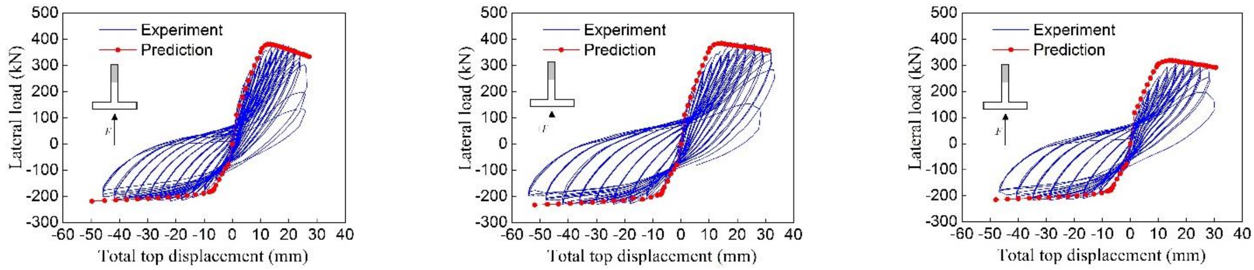

(a) TW-1 (b) TW-3 (c) TW-4

Fig. 11 Comparison of predicted lateral load-top displacement skeleton curves to experimental hysteretic curves

assumed cracking angle of 45 degrees is smaller than the experimental observed one, which results in the underestimation of the proportional constant C and the shear displacements. In general, the proposed model can reasonably predict the shear deformation response of flanged walls.

5. Evaluation of the integrated model

By integrating the deformations due to flexure, shear, and strain penetration, a new load-deformation analytical model is proposed for flexure-dominant flanged walls. Fig. 11 shows the envelopes derived from the integrated model in comparison to the experimental force-displacement hystereses for all three test specimens. The results show that the predicted response of both specimens in the flange-in-tension and flange-in-compression loading directions captures the shape of the measured response envelope reasonably well, which illustrates that the integrated model proposed in this paper can predict the load-deformation response of flanged walls with sufficient accuracy.

The proposed model provides engineers with a simple, accurate modeling tool appropriate for routine design work. Through simple sectional analysis, the effects of the axial load ratio, reinforcement content, material properties and geometric parameters on the deformation behavior of flanged walls can be quantified in the proposed model. In addition, the monotonic pushover curve can be determined directly by substituting the design parameters and the moment-curvature response into the proposed formulas, without requiring a complex iteration process. Furthermore, to ensure the accuracy and wide applicability of the model, purely empirical relationships and oversimplified assumptions are avoided as much as practical. The proposed modeling procedure is applicable not only to the T-shaped RC walls studied in this paper but also to rectangular walls and other flanged walls with arbitrary sections. However, for asymmetrical flanged walls, moment-curvature analyses should be conducted in both flange-in-tension and flange-in-compression loading directions.

Given the differences in the profiles of shear displacement and flexural displacement over the wall height, the existing models for predicting the shear deformation as a constant fraction of flexural deformation can only estimate the shear displacement at the top of the wall. Applying a multiplier for estimating the shear displacements at other positions will lead to underestimation in the plastic hinge region and overestimation in the elastic region. For the model proposed in this paper, a more realistic proportional relationship between shear displacement and flexural rotation is established according to the similar gross shapes of the curvature and shear strain distributions over the wall height.

Therefore, this model can be used to predict the shear displacement and total deformation at any position over the wall height, and the derived displacement profile is of great significance to the direct displacement-based design procedure.

The integrated model can predict the monotonic pushover curves of flexure-dominant RC walls very well, explicitly accounting for each of the flexural, shear, and strain penetration components of deformation. However, several shortcomings still exist in the proposed model. First, because the model is based on a flexural section analysis that assumes that plane sections remain plane, the shear lag effects are neglected in the calculation. However, the shear lag effects may have less influence on the deformation behavior of flexure-dominant walls. Second, the tension shifting effects are neglected in the model, which leads to a reduced prediction of plastic hinge length and underestimation of the deformation in the plastic range; however, this underestimation tends to be conservative for design purposes. Third, when calculating the cracked shear stiffness using the truss model, the cracking angle is assumed to be 45 degrees for the sake of simplicity, which deviates from the true cracking angle especially for the T-shaped walls with the flange in compression. A better estimation of the cracking angle can be obtained by the equation from Collins and Mitchell (1997). Generally, the proposed integrated model can give good prediction of the load-deformation response of flexure-dominant RC walls.

6. Simplified calculation of ultimate displacement

Ultimate displacement capacity is an important index that determines the ductility and energy dissipation capacity of a structure and is critical to performance-based seismic designs and seismic capacity evaluations. The ultimate displacement (curvature) is defined as the smallest value in the following three cases: (1) the moment resistance decreases to 85% of the maximum moment capacity; (2) the core concrete achieves the ultimate compressive strain of 0.018; (3) the longitudinal tensile bars achieve the ultimate tensile strain of 0.06 (Smyrou *et al.* 2013).The analytical model established above can be used to predict the ultimate displacement capacity of flanged walls based on a flexural section analysis. However, given that most of the time only the ultimate displacement is needed, it is necessary to establish a simpler procedure without section analysis for estimating the ultimate displacement capacity of flanged walls.

6.1 Estimation of ultimate flexural displacement capacity

Following the method for calculating the flexural deformation of the wall panel in Section 3.1, the ultimate flexural displacement of flanged walls can be estimated using the plastic hinge model as follows:

$$\Delta_{fu} = \frac{1}{3}\phi_y H^2 + (\phi_u - \phi_y) l_p H \tag{17}$$

where the yield curvature ϕ_y and the ultimate curvature ϕ_u can be determined from the author's early research on curvature estimation of asymmetrical flanged walls (Wang *et al.* 2019b). For the case with the flange in tension, the yield curvature and ultimate curvature can be calculated as follows:

$$\phi_{yFiT} = \frac{\varepsilon_y}{l_w}(2.77 - 3.66n + 11.17\rho - 0.49\frac{b_f}{l_w}) \tag{18}$$

$$\phi_{uFiT} = \frac{1}{1000 l_w}(37.94 + 37.73e^{-8.83n} - 751.68\rho - 11.33\frac{b_f}{l_w} + 804.56\rho_v - 1.36\frac{l_w}{t}) \tag{19}$$

For the case with the flange in compression, the yield curvature and ultimate curvature can be calculated as follows:

$$\phi_{yFiC} = \frac{\varepsilon_y}{l_w}(1.61 + 8.91\rho + 14.92\rho_w) \tag{20}$$

$$\phi_{uFiC} = \frac{1}{1000 l_w}(68.65 + 12.67n - 2.31\frac{b_f}{l_w} - 0.27\frac{l_w}{b_w}) \tag{21}$$

where ε_y is the steel yield strain, l_w is the web height, n is the axial load ratio, ρ is the boundary longitudinal reinforcement ratio, ρ_w is the web distributed vertical reinforcement ratio, ρ_v is the transverse reinforcement ratio, and b_f is the flange width.

Since the section analysis is no longer performed in the simplified calculation of ultimate displacement, the equivalent plastic hinge length used for estimating the flexural deformation of the wall panel cannot be determined based on the moment of each loading step derived from the moment-curvature analysis as in Eq. (2). Moreover, for the estimation of the flexural deformation due to strain penetration, Eq. (7) is also no longer applicable because the maximum strain in the extreme tensile bars and the neutral axis depth at the ultimate limit state are not known. Therefore, combining the contributions of the above two types of flexural deformations, the total flexural deformation can be calculated through a unified equivalent plastic hinge length. Considering the contributions of moment gradient and strain penetration to the spread of plasticity, Paulay and Priestley (1992) proposed the following expression to estimate the total equivalent plastic hinge length of shear walls:

$$l_{pFIC} = 0.08H + 0.022 d f_y \tag{22}$$

where the first term represents the spread of plasticity due to moment gradient and the second term represents the increased rotation capacity due to strain penetration. Eq. (22) is applicable to asymmetrical flanged walls with the flange in compression because such walls have similar mechanical behaviors to ordinary rectangular walls. However, for the case with the flange in tension, as the stiff flange prevents the diagonal cracks and the plasticity from spreading, the plastic hinge length in this loading direction is relatively smaller than that in the flange-in-compression loading direction. A comparison with the experimental results shows that improved predictions of the equivalent plastic hinge length in

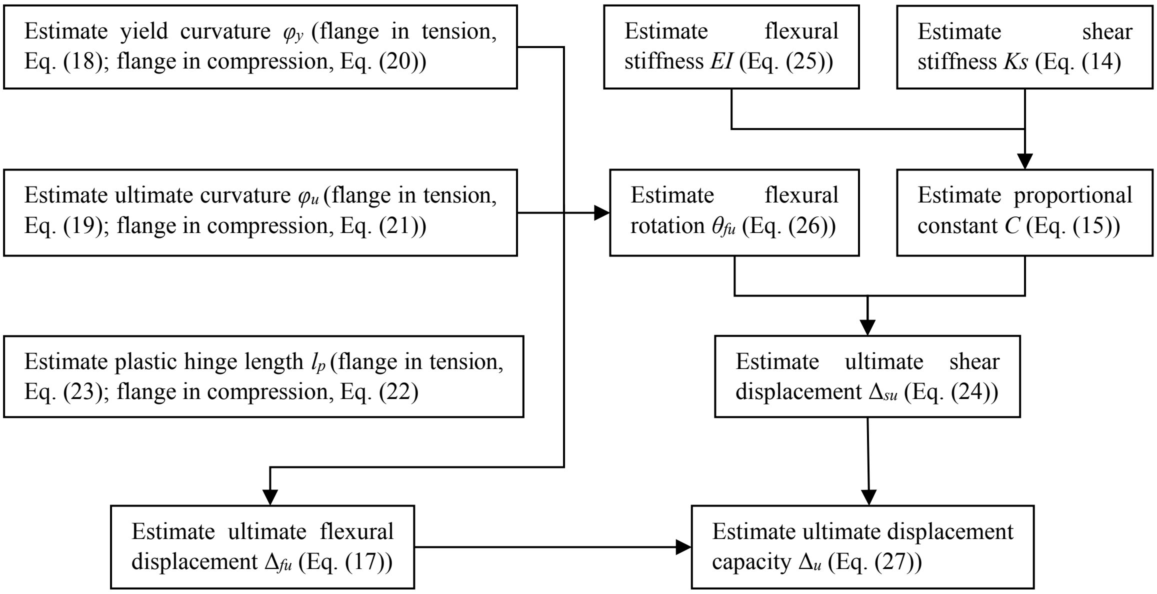

Fig. 12 Flow chart for estimating the ultimate displacement capacity

the flange-in-tension loading direction can be obtained by modifying Eq. (22) to the following expression:

$$l_{pFIT} = 0.06H + 0.022df_y \tag{23}$$

6.2 Estimation of the ultimate shear displacement capacity

Following the proportional relationship between shear displacement and flexural rotation established in Section 3.2, the ultimate shear displacement of flanged walls can be estimated as follows:

$$\Delta_{su} = C\theta_{fu} \tag{24}$$

However, when using Eq. (13) to calculate the proportional constant C, the flexural stiffness at first yielding can no longer be determined using the yield moment and yield curvature derived from the moment-curvature analysis. Therefore, the flexural stiffness can be approximately determined based on the method for predicting the short-term stiffness of cracked concrete from the Chinese code for design of concrete structures (GB 50010, 2010) as follows:

$$EI = \frac{E_s A_s h_0^2}{1.15\psi + 0.2 + \dfrac{6a_E\rho}{1+3.5\gamma'_f}} \tag{25}$$

where ψ is the non-uniformity coefficient for the strain of the longitudinal tensile reinforcement between cracks (for cyclic loading ψ=1); $\gamma' f$ is the ratio of the cross-sectional area of the compressive flange to the effective cross-sectional area of the web, which can be estimated as $\gamma'_\mathrm{f} = (b_\mathrm{f} - b_\mathrm{w})h_\mathrm{f} / b_\mathrm{w}h_0$; and A_s is the cross-sectional area of the longitudinal tensile reinforcement. The cracked shear stiffness per length can still be calculated by Eq. (14), and the ultimate flexural rotation can be estimated using the plastic hinge model as follows:

$$\theta_{fu} = \frac{1}{2}\phi_y H + (\phi_u - \phi_y)l_p \tag{26}$$

6.3 Procedure for estimating the ultimate displacement capacity

The ultimate displacement capacity of flanged walls can be obtained by summing the flexural and shear components of deformation:

$$\Delta_u = \Delta_{fu} + \Delta_{su} \tag{27}$$

The specific procedure for estimating the ultimate displacement is shown in Fig. 12.

Table 5 compares the ultimate displacements predicted using the procedure established above to the experimental results of the asymmetrical flanged walls tested by the author (Wang *et al.* 2018) and Thomsen and Wallace (2004). The predicted values differ within 10% from the measured values of the specimens tested by the author. However, a relatively large discrepancy exists in the specimens tested by Thomsen and Wallace. The predicted values of the ultimate displacement are larger than the measured values for specimen TW1, especially for the case with the flange in compression. This overestimation occurs because specimen TW1 exhibited a brittle failure and failed to reach the nominal moment due to the poor detailing provided at the web boundary. The predicted ultimate displacements of specimen TW2 are in good agreement with the measured values when the flange was in compression but are smaller than the measured values when the flange was in tension. The reason for the large discrepancy in the comparison for specimen TW2 is that the

Table 5 Comparison between measured and predicted ultimate displacements

	Specimen	Δ_u (flange in tension)			Δ_u (flange in compression)		
		Measured (mm)	Predicted (mm)	Difference (%)	Measured (mm)	Predicted (mm)	Difference (%)
Wang *et al.* (2018)	TW-1	28.85	26.82	7.05	43.39	47.30	-9.02
	TW-2	27.93	26.82	3.97	44.42	47.30	-6.47
	TW-3	33.03	29.96	9.28	53.08	49.74	6.30
	TW-4	29.16	26.98	7.47	46.95	47.23	-0.59
	LW-1	29.36	26.65	9.24	46.65	47.28	-1.35
Thomsen and Wallace (2004)	TW-1	45.44	49.94	-9.90	58.70	92.72	-57.96
	TW-2	82.17	65.66	20.09	88.90	90.99	-2.35

spacing of the transverse reinforcement used at the web boundary is as small as 32 mm, which exceeds the range of curvature estimation in the author's early research, resulting in the underestimation of the ultimate curvature. However, the hoop spacing of 32 mm is seldom used in practical engineering applications due to its inconvenience in construction. In general, the simplified procedure proposed in this paper can estimate the ultimate displacement capacity of flanged walls with sufficient accuracy. Nevertheless, given that few well- documented experimental data are available to assess the ultimate displacement of asymmetrical flanged walls in both the flange-in-tension and flange-in-compression loading directions, further experimental investigations are needed for additional verification.

7. Conclusions

Experimental results for three mid-rise T-shaped RC walls are presented to identify the relative contributions of the flexural, shear and sliding deformations to the lateral displacements at different loading stages. Results of the tests indicate that the shear deformations can contribute more than 15% of the total displacement and the ratio of shear-to-total top displacements remains approximately constant over the entire plastic range. The sliding deformations contribute less than 3% of the total displacement and can be neglected in the calculation of the deformation capacity.

Based on the observed deformation behavior, a new load-deformation analytical model is proposed for flexure-dominant flanged walls, in which each of the three components of wall deformation (flexure, shear, and strain penetration) is modeled separately. Flexural deformations are estimated from a modified plastic hinge model that considers the changes in plastic hinge length.

Deformations due to strain penetration are estimated from a simplified mechanics-based model that facilitate the determination of anchorage length and strain distribution of the tensile bars. Shear deformations are estimated from the derived flexural rotation, and the proportional constant between them can be determined according to the truss model and the observation that the shear-to-flexural displacement ratio is independent of the top displacement demand.

A detailed verification of the analytical models is provided by comparing with the experimental results at the global and component scales. It is concluded that the integrated model provides engineers with a simple, accurate modeling tool to capture the load-deformation responses of flanged walls. Compared to conventional analytical models, the proposed model can predict the monotonic pushover curve without a complex iteration process, and purely empirical relationships and oversimplified assumptions are avoided as much as practical. In addition, through simple sectional analysis, the effects of the axial load ratio, reinforcement content, material properties and geometric parameters on the deformation behavior of flanged walls can be quantified in the model. The proposed model can further be applied to flexural walls with arbitrary sections and is capable of determining displacements at any position over the wall height, which is of great significance to the direct displacement-based design procedure.

To rapidly and accurately evaluate the deformation capacity of flanged walls, a simple procedure for estimating the ultimate displacement capacity is proposed by simplifying the analytical model, which will be valuable for performance-based seismic designs and seismic capacity evaluations.

Acknowledgments

The work presented in this paper was supported by the National Natural Science Foundation of China (grant numbers 51808435 and 51878540), the Natural Science Foundation of Shaanxi Province (grant number 2019JQ-199), the China Postdoctoral Science Foundation (grant number 2018M643594), and the Young Talent fund of University Association for Science and Technology in Shaanxi Province (grant number 20190419); these financial supports are gratefully acknowledged.

References

Bafti, F.G., Mortezaei, A. and Kheyroddin, A. (2019). “The length of plastic hinge area in the flanged reinforced concrete shear walls subjected to earthquake ground motions”, *Struct. Eng. Mech.*, **69**(6), 651–665. https://doi.org/10.12989/SEM.2019.69.6.651.

Beyer, K., Dazio, A. and Priestley, M.J.N. (2008), “Quasi-static cyclic tests of two U-shaped reinforced concrete walls”, *J.*

Earthq. Eng., **12**(7), 1023-1053. https://doi.org/10.1080/13632460802003272.

Beyer, K., Dazio, A. and Priestley, M.J.N. (2011), "Shear deformations of slender reinforced concrete walls under seismic loading", *ACI Struct. J.*, **108**(2), 167-177. https://doi.org/10.14359/51664252.

Brueggen, B.L. (2009), "Performance of T-shaped reinforced concrete structural walls under multi-directional loading", Ph.D. Dissertation, University of Minnesota, Minnesota.

Chen, Z., Xu, J., Chen, Y. and Su, Y. (2016), "Seismic behavior of T-shaped steel reinforced high strength concrete short-limb shear walls under low cyclic reversed loading", *Struct. Eng. Mech.*, **57**(4), 681-701. https://doi.org/10.12989/sem.2016.57.4.681.

Choi, C.-S., Ha, S.-S., Lee, L.-H., Oh, Y.-H. and Yun, H.-D. (2004), "Evaluation of deformation capacity for RC T-shaped cantilever walls", *J. Earthq. Eng.*, **8**(3), 397-414. https://doi.org/10.1080/13632460409350494.

Collins, M.P. and Mitchell, D. (1997), *Prestressed Concrete Structures*, Response Publications, Toronto, ON.

Dang, Z., Liang, X. and Yu, J. (2014), "Nonlinear analysis of axial-flexure-shear coupling behavior of fiber reinforced concrete shear walls", *J. Build. Struct.*, **35**, 104-112. https://doi.org/ 10.14006/j.jzjgxb.2014.08.036.

Dazio, A., Wenk, T. and Bachmann, H. (1999), *Quasi-Static Cyclic Tests on RC Structural Walls*. Report No. 239, ETH, Zurich, Switzerland.

Eligehausen, R., Popov, E.P. and Bertero, V.V. (1983), "Local Bond Stress-Slip Relationships of Deformed Bars under Generalized Excitations", Research Report No. UCB/EERC-83/23; Energy Environmental Research Center, University of California, Berkeley, California, USA.

Grammatikou, S., Biskinis, D. and Fardis, M.N. (2015), "Strength, deformation capacity and failure modes of RC walls under cyclic loading", *Bull Earthq Eng*., **13**(11), 3277-3300. https://doi.org/10.1007/s10518-015-9762-x

Hines, E.M. (2002), "Seismic performance of hollow rectangular reinforced concrete bridge piers with confined corner elements", Ph.D. Thesis, University of California, San Diego.

Hines, E.M., Restrepo, J.I. and Seible, F. (2004), "Force-displacement characterization of well-confined bridge piers", *ACI Struct. J.*, **101**(4), 537-548. https://doi.org/10.14359/13340.

Hossain, K.M. Anwar and Wright, H.D. (2004). "Flexural and shear behaviour of profiled double skin composite elements", *Steel Compos. Struct.*, **4**(2), 113–132. https://doi.org/10.12989/SCS.2004.4.2.113

Hua, J. and Yahya, C.K. (2010), "Analytical modeling of medium-rise reinforced concrete shear walls", *ACI Struct. J.*, **107**(4), 400-410. https://doi.org/10.14359/51663812.

Kabir, M.Z. and Vasheghani-Farahani, R. (2009). "Experimental investigation of performance in L-shaped wall to wall corner connections of 3D Panels subjected to lateral cyclic loading", *Struct. Eng. Mech.*, **33**(5), 649-652. https://doi.org/10.12989/SEM.2009.33.5.649

Kang, S.-M. and Kim, J.Y. (2014), "Evaluation of deformation capacity including yield deformation in displacement-based design of special RC shear wall", *Struct. Design Tall Spec. Build.*, **23**(3), 181-209. https://doi.org/10.1002/tal.1030.

Lowes, L.N. and Altoontash, A. (2003), "Modeling reinforced-concrete beam-column joints subjected to cyclic loading", *J. Struct. Eng.*, **129**(12), 1686-1697. https://doi.org/10.1061/(asce)0733-9445(2003)129:12(1686).

Lu, Y.Q. and Huang, L. (2014). "Experimental study on cyclic behavior of reinforced concrete parallel redundancy walls", *Struct. Eng. Mech.*, **52**(6), 1177-1191. https://doi.org/10.12989/SEM.2014.52.6.1177

Massone, L.M. and Alfaro, J.I. (2016), "Displacement and curvature estimation for the design of reinforced concrete slender walls", Struct. Design Tall Spec. Build., **25**(16), 823-841. https://doi.org/10.1002/tal.1285.

Massone, L.M., Orakcal, K. and Wallace, J.W. (2006), Shear-flexure interaction for structural walls, In: Motomoros, A. and Elwood, K. *Deformation Capacity and Shear Strength of Reinforced Concrete Members under Cyclic Loading,* ACI Special Publication, pp. 127-150.

Mostafaei, H. and Vecchio, F.J. (2008), "Uniaxial shear-flexure model for reinforced concrete elements", *J. Struct. Eng.*, **134**(9), 1538-1547. https://doi.org/10.1061/(asce)0733-9445(2008)134:9(1538).

Park, R. and Paulay, T. (1975), *Reinforced Concrete Structures,* John Wiley & Sons, New York.

Parulekar, Y.M., Reddy, G.R., Singh, R.K., Gopalkrishnan, N. and Ramarao, G.V. (2016). "Seismic performance evaluation of mid-rise shear walls: experiments and analysis", *Struct. Eng. Mech.*, **59**(2), 291–312. https://doi.org/10.12989/SEM.2016.59.2.291

Paulay, T. and Priestley, M.J.N. (1992), *Seismic Design of Reinforced Concrete and Masonry Buildings*, John Wiley & Sons, New York.

Priestley, M.J.N., Calvi, G.M. and Kowalsky, M.J. (2007), *Displacement-Based Seismic Design of Structures*, IUSS Press, Pavia, Italy.

Sakr, M.A., El-khoriby, S.R., Khalifa, T.M. and Nagib, M.T. (2017). "Modeling of RC shear walls strengthened by FRP composites", *Struct. Eng. Mech.*, **61**(3), 407-417. https://doi.org/10.12989/SEM.2017.61.3.407

Shi, Q.X. and Liang, X.W. (2012), *Design of Tall Building Structures*, Science Press, Beijing, China.

Smyrou, E., Sullivan, T., Priestley, N. and Calvi, M. (2013) "Sectional response of T-shaped RC walls", *Bull Earthquake Eng.*, **11**(4), 999-1019. https://doi.org/10.1007/s10518-012-9407-2.

Takahashi, S., Yoshida, K., Ichinose, T., Sanada, Y., Matsumoto, K., Fukuyama, H. and Suwada, H. (2013), "Flexural drift capacity of reinforced concrete wall with limited confinement", *ACI Struct. J.*, **110**(1), 95-104. https://doi.org/10.14359/51684333.

Thomsen, J.H. and Wallace, J.W. (2004), "Displacement-based design of slender reinforced concrete structural walls—experimental verification", *J. Struct. Eng.*, **130**(4), 618-630. https://doi.org/10.1061/(asce)0733-9445(2004)130:4(618).

Varughese, J.A., Menon, D. and Prasad A.M. (2015), "Displacement-based seismic design of open ground storey buildings", *Struct. Eng. Mech.*, **54**(1), 19-33. https://doi.org/10.12989/sem.2015.54.1.019.

Wang, B., Shi, Q.X. and Cai, W.Z. (2018), "Seismic behavior of flanged reinforced concrete shear walls under cyclic loading", *ACI Struct. J.*, **115**(5), 1231-1242. https://doi.org/10.14359/51702379.

Wang, B., Shi, Q.X. and Cai, W.Z. (2019), "Decoupling and analysis of the deformation of flanged reinforced concrete shear walls", Struct. Design Tall Spec. Build., **28**(13), e1628. https://doi.org/10.1002/tal.1628.

Wang, B., Cai, W.Z. and Shi, Q.X. (2019b), "Simplified data-driven model for the moment curvature of T-shaped RC shear walls", *Adv Civ Eng.*, 9897827. https://doi.org/10.1155/2019/9897827.

Zhang, S.L. Lu, X.L. and Zhang, H.M. (2009), "Experimental and analytical studies on the ultimate displacement of RC shear walls", *China Civil Eng. J.*, **42**(4), 10-16. https://doi.org/10.15951/j.tmgcxb.2009.04.007.

Zhao, H.J., Li, Q.N., Song, C., Jiang, H.T. and Zhao, J. (2017). "Seismic tests of RC shear walls confined with high-strength rectangular spiral reinforcement", *Steel Compos. Struct.*, **24**(1), 1-13. https://doi.org/10.12989/SCS.2017.24.1.001.

Zhao, J. and Sritharan, S. (2007), "Modeling of strain penetration effects in fiber-based analysis of reinforced concrete structures", *ACI Struct. J.*, **104**(2): 133-141. https://doi.org/10.14359/18525.

Zhou, Y., Zhang, D., Huang, Z. and Li, D. (2014), "Deformation capacity and performance-based seismic design for reinforced concrete shear walls", *J. Asian Archit. Build. Eng.*, **13**(1), 209-215. https://doi.org/10.3130/jaabe.13.209.

PL